Magnetic Nanocomposites: Preparation and Characterization of Polymer-Coated Iron Nanoparticles

Nicholas A. D. Burke,[†] Harald D. H. Stöver,*[,†] and Francis P. Dawson[‡]

Department of Chemistry, McMaster University, Hamilton, Ontario, Canada L8S 4M1, and Department of Electrical and Computer Engineering, University of Toronto, Toronto, Ontario, Canada M5S 3G4

Received May 20, 2002

Nanoparticles bearing a strongly bound polymer coating were formed by the thermal decomposition of iron pentacarbonyl in the presence of ammonia and polymeric dispersants. The dispersants consist of polyisobutylene, polyethylene, or polystyrene chains functionalized with tetraethylenepentamine, a short polyethyleneimine chain. Polystyrene-based dispersants were prepared with both graft and block copolymer architectures. Inorganic−organic core−shell nanoparticles were formed with all three types of dispersants. In addition, more complex particles were observed in the case of the polystyrene-based dispersants in 1-methylnaphthalene. The core material was identified as metallic iron, while the particle shells are formed from the polymeric dispersant which binds to the core. High-resolution TEM revealed evidence for crystallization within the polymer shell, possibly facilitated by chain alignment upon binding. The nanocomposites display room-temperature magnetic behavior ranging from superparamagnetic to ferromagnetic. The saturation magnetization and coercivity were found to depend on the diameter of the iron core.

Introduction

Nanoparticle materials have become the focus of increasing attention because the physical properties often differ significantly from those of the corresponding bulk material.[1−8] In solution, nanoparticles are typically prepared from soluble precursors, and some means of limiting particle growth is required to obtain small particle sizes. Transformation of the soluble precursors into the nanoparticle material has been accomplished by means such as thermal[6,8−14] or sonochemical[15−18] decomposition and electrochemical[19] or chemical reduction.[6,20] Particle growth is controlled by restricting particle formation to confined volumes such as micelles[21] and vesicles[22] or by stabilizing the growing particle with surfactants or dispersants.[6,9−18,20d] If an organic material is used to limit particle growth and it is isolated with the magnetic material, an inorganic−organic nanocomposite can be obtained.

The work described in this paper deals with iron−polymer magnetic nanocomposites. Magnetic nanoparticles, such as those formed from iron, have fascinating magnetic properties that have fueled both fundamental and applied studies.[2,5−18,23] Iron nanoparticles are normally prepared by the thermal or sonochemical decomposition of iron pentacarbonyl,[6,9,12,13,15−18] and aggregation of the particles is often minimized by adding surfactants/dispersants. For example, Suslick et al.[15] found that the presence of oleic acid or poly(vinylpyrrolidone) during the sonochemical decomposition of iron

* To whom correspondence should be addressed.
[†] McMaster University.
[‡] University of Toronto.

(1) *Clusters and Colloids, from Theory to Applications*; Schmid, G., Ed.; VCH: New York, 1994.
(2) Leslie-Pelecky, D. L.; Rieke, R. D. *Chem. Mater.* **1996**, *8*, 1770.
(3) Rao, C. N. R.; Kulkarni, G. U.; Thomas, J. P.; Edwards, P. P. *Chem. Soc. Rev.* **2000**, *29*, 27.
(4) Alivisatos, A. P. *Science* **1996**, *271*, 933.
(5) Easom, K. A.; Klabunde, K. J.; Sorensen, C. M.; Hadjipanayis, G. C. *Polyhedron* **1994**, *13*, 1197.
(6) Sun, S.; Murray, C. B.; Weller, D.; Folks, L.; Moser, A. *Science* **2000**, *287*, 1989.
(7) Tejada, J.; Zhang, X. X.; Kroll, E.; Bohigas, X.; Ziolo, R. F. *J. Appl. Phys.* **2000**, *87*, 8008.
(8) MacLachlan, M. J.; Ginzburg, M.; Coombs, N.; Coyle, T. W.; Raju, N. P.; Greedan, J. E.; Ozin, G. A.; Manners, I. *Science* **2000**, *287*, 1460.
(9) Nakatani, I.; Hijikata, M.; Ozawa, K. *J. Magn. Magn. Mater.* **1993**, *122*, 10.
(10) Thomas, J. R. *J. Appl. Phys.* **1966**, *37*, 2914.
(11) Hess, P. H.; Parker, P. H., Jr. *J. Appl. Polym. Sci.* **1966**, *10*, 1915.
(12) Smith, T. W.; Wychick, D. *J. Phys. Chem.* **1980**, *84*, 1621; Griffiths, C. H.; O'Horo, M. P.; Smith, T. W. *J. Appl. Phys.* **1979**, *50*, 7108.
(13) Tannenbaum, R.; Flenniken, C. L.; Goldberg, E. P. *J. Polym. Sci., Part B*: *Polym. Phys.* **1990**, *28*, 2421.
(14) Bronstein, L. M.; Mirzoeva, E. S.; Valetsky, P. M.; Solodovnikov, S. P.; Register, R. A. *J. Mater. Chem.* **1995**, *5*, 1197.
(15) Suslick, K. S.; Fang, M.; Hyeon, T. *J. Am. Chem. Soc.* **1996**, *118*, 11960.
(16) Wizel, S.; Margel, S.; Gedanken, A. *Polym. Int.* **2000**, *49*, 445.
(17) Wizel, S.; Margel, S.; Gedanken, A.; Rojas, T. C.; Fernández, A.; Prozorov, R. *J. Mater. Chem.* **1999**, *14*, 3913.
(18) Wizel, S.; Prozorov, R.; Cohen, Y.; Aurbach, D.; Margel, S.; Gedanken, A. *J. Mater. Chem.* **1998**, *13*, 211.
(19) Weisshaar, D. E.; Kuwana, T. *J. Electroanal. Chem.* **1984**, *163*, 395.
(20) (a) Vidoni, O.; Philippot, K.; Amiens, C.; Chaudret, B.; Balmes, O.; Malm, J.-O.; Boivin, J.-O.; Senocq, F.; Casanove, M.-J. *Angew. Chem., Int. Ed.* **1999**, *38*, 3736. (b) Perez, H.; Pradeau, J.-P.; Albouy, P.-A.; Perez-Omil, J. *Chem. Mater.* **1999**, *11*, 3460. (c) Hashimoto, T.; Harada, M.; Sakamoto, N. *Macromolecules* **1999**, *32*, 6867. (d) Ely, T. O.; Amiens, C.; Chaudret, B.; Snoeck, E.; Verelst, M.; Respaud, M.; Broto, J.-M. *Chem. Mater.* **1999**, *11*, 526.
(21) Kommareddi, N. S.; Tata, M.; John, V. T.; MacPherson, G. L.; Herman, M. F.; Lee, Y.-S.; O'Connor, C. J.; Akkara, J. A.; Kaplan, D. L. *Chem. Mater.* **1996**, *8*, 801.
(22) Yaacob, I. I.; Nunes, A. C.; Bose, A. *J. Colloid Interface Sci.* **1995**, *171*, 73.
(23) Odenbach, S. *Adv. Colloid Interface Sci.* **1993**, *46*, 263.

10.1021/cm020126q CCC: $22.00
Published on Web 10/09/2002

pentacarbonyl leads to the formation of stable colloidal dispersions of iron nanoparticles. Sun et al.[6] were able to produce monodisperse FePt nanoparticles by coupling the thermolysis of iron pentacarbonyl with the reductive decomposition of $Pt(acac)_2$ in the presence of oleic acid and oleylamine.

Polymers with a wide variety of compositions, structures, and properties are available, which makes them ideal components for nanocomposite materials. Polymer composites containing ferromagnetic materials such as iron,[9,12,13,15−18] cobalt,[10,11,13,14,17] and nickel[19] have been reported. In these polymer−metal composites, the polymer is often only weakly bound to the metal particles, if at all. Dispersants with a head−tail structure and a strongly binding headgroup may be able to bind more securely and densely on the metal surface.

Nakatani et al.[9] have used a polymeric dispersant with a head−tail structure during the formation of iron nitride nanoparticles. The polymer, a soot dispersant in automotive oils, had a block copolymer structure with a long polyisobutylene chain joined at one end to a shorter tetraethylenepentamine chain. ϵ-Fe_3N, which is more resistant to oxidation than iron, was obtained in the form of fairly uniform nanoparticles dispersed in hydrocarbon solvents. Polyisobutylene likely forms a protective coating around each particle, although this coating was not directly detected.

We sought to extend this approach to the preparation of core−shell nanoparticles with well-defined shells composed of polyisobutylene, polyethylene, or polystyrene. The dispersant will determine the nature and thickness of the polymer shell, which could in turn affect nanocomposite properties such as particle size and morphology, solubility, and melting behavior. In addition, the polymer shell may protect the core against degradation or allow the formation of close-packed particle arrays with a fixed interparticle spacing. The syntheses of a polyethylene dispersant and a series of polystyrene dispersants of both block and graft architectures are described. These dispersants, plus a commercially available polyisobutylene-based one, were used to prepare hybrid nanoparticles where each iron-based core bears a strongly bound polymer coating. The structural characterization and magnetic properties of these materials are presented.

Experimental Section

General. Iron pentacarbonyl, kerosene, 1-methylnaphthalene, Decalin, tetraethylenepentamine (TEPA), benzoyl peroxide, styrene, 4-vinylbenzyl chloride, (1-bromoethyl)benzene, 2,2′-dipyridyl, copper(I) bromide, and poly(ethylene-*graft*-maleic anhydride) (3 wt % maleic anhydride) were purchased from Aldrich Chemical Co. (Oakville, ON). Toluene, acetone, and hexanes (Caledon Laboratories, Georgetown, ON), methanol and xylenes (Anachemia, Montreal, QC), and ammonia gas and argon (Canadian Liquid Air, Hamilton, ON) were used as received. A dispersant comprised of polyisobutylene functionalized with tetraethylenepentamine (PIB−TEPA) as a 1:1 mixture with mineral oil was generously provided by Imperial Oil (now Esso Research, Sarnia, ON).

Nuclear magnetic resonance spectra were measured with a Bruker AC-200 (200 MHz) on samples dissolved in deuteriochloroform. Polymer molecular weights were determined by size exclusion chromatography utilizing three 30-cm Waters Ultrastyragel Linear columns with THF as the eluent. Glass transition temperatures (T_g) were measured by differential scanning calorimetry (TA Instruments DSC-2910). Samples were heated to 160 °C, quenched by removing the sample from the hot DSC cell, and then scanned a second time with a 10 °C/min temperature ramp. T_g was taken as the midpoint of the transition region in this second scan. Thermogravimetric analyses were performed under an argon atmosphere with a Netsch STA 409. Infrared spectra were measured from thin films with a Bio-Rad FTS-40 FTIR. Elemental analyses were performed by Guelph Chemical Laboratories (Guelph, ON). Iron content was determined by ICP-MS performed at the School of Geology and Geography, McMaster University. Magnetic measurements were performed with a Quantum Design MPMS SQUID magnetometer at 17 °C.

Samples for TEM analysis were prepared by placing a drop of a toluene or hexane dispersion of the nanoparticles (0.1−0.5 wt %) on a carbon-coated copper TEM grid and allowing the solvent to evaporate. TEM analysis was performed with a Philips CM12 operating at 120 kV or a JEOL JEM-2010F operating at 200 kV. Particle sizes were measured directly from the images or by analysis of digitized images with ImageTool software (UTHSCSA). Particle sizes are reported as the mean ± the standard deviation measured from 100 or more particles. Polycrystalline gold, partially coating some samples, was used to calibrate *d* spacings obtained from electron diffraction patterns.

Poly(styrene-*graft*-tetraethylenepentamine) (PS-*g*-TEPA) Dispersants. Styrene (49.64 g, 476.6 mmol), 4-vinylbenzyl chloride (0.38 g, 2.5 mmol), and benzoyl peroxide (0.42 g, 1.73 mmol) were dissolved in 200 mL of toluene in a 500-mL, two-necked round-bottom flask fitted with a condenser. The solution was deoxygenated by bubbling with argon for 30 min and then heated to 80 °C for 24 h and 100 °C for 4 h. A sample of the reaction mixture (3 g, ∼1.3%) was removed before the addition of tetraethylenepentamine (TEPA, 5.00 g, 26 mmol) dissolved in toluene (10 mL). Heating to 85 °C caused the solution to go cloudy after ∼30 min. After 20 h at 85 °C, the mixture was cooled and the toluene solution containing PS-*g*-TEPA was separated from the yellow oil that had settled from the reaction mixture. PS-*g*-TEPA and the small sample of poly(styrene-*co*-4-vinylbenzyl chloride) (PS−VBC) removed after the initial polymerization were each isolated and purified by two precipitations in methanol. The white solids were air-dried and then further dried for 24 h in a vacuum oven at 60 °C to yield 34.1 g (68% overall) of PS-*g*-TEPA ($M_n = 1.6 \times 10^4$ g/mol; $T_g = 93$ °C) and 0.39 g (58%) of PS−VBC ($M_n = 3.2 \times 10^4$ g/mol; $T_g = 102$ °C). Other PS-*g*-TEPA dispersants were prepared in a similar manner.

Poly(styrene-*block*-tetraethylenepentamine) (PS-*b*-TEPA) Dispersants. Styrene (50.01 g, 480 mmol), (1-bromoethyl)benzene (0.46 g, 2.5 mmol), copper(I) bromide (0.36 g, 2.5 mmol), 2,2′-dipyridyl (1.17 g, 7.5 mmol), and copper (0.08 g, 1.3 mmol) were placed in a 100-mL round-bottom flask. The solution was deoxygenated by bubbling with argon for 30 min and then the flask was immersed in a 110 °C oil bath for 4.5 h. The reaction mixture, a viscous oil, was dissolved in toluene and filtered through glass wool to remove precipitated copper salts. Polystyrene was then isolated from the toluene by precipitation in methanol and further purified by an additional precipitation from toluene into methanol. The white solid was dried to yield 32.25 g (64%) of bromine-terminated polystyrene ($M_n = 2.0 \times 10^4$ g/mol; $T_g = 96$ °C).

TEPA (3.5 g, 18.5 mmol) dissolved in 10 mL of toluene was added to a solution of bromine-terminated polystyrene (31.86 g, 1.6 mmol of Br) dissolved in 200 mL of toluene. The mixture was heated to 85 °C, at which point it went cloudy. After 16 h at ∼85 °C, the solution was cooled and the toluene solution containing PS-*b*-TEPA was separated from the oil that had settled from the reaction mixture. PS-*b*-TEPA was isolated and purified by two precipitations in methanol. The white solid was air-dried and then dried for 24 h in a vacuum oven at 60 °C to yield 30.0 g (94% for this step or 60% overall) of PS-*b*-TEPA ($M_n = 1.9 \times 10^4$ g/mol; $T_g = 94$ °C). Other PS-*b*-TEPA dispersants were prepared in a similar manner.

Poly(ethylene-*graft*-tetraethylenepentamine maleimide) (PE-*g*-TEPA) Dispersant. Polyethylene grafted with 3%

maleic anhydride (50.00 g, 15.3 mmol of anhydride) and xylenes (200 mL) were placed in a 500-mL round-bottom flask fitted with a Dean−Stark head. The mixture was heated to dissolve the polymer before tetraethylenepentamine (14.5 g, 76.6 mmol) dissolved in 15 mL of xylene was added rapidly. The reaction mixture was then refluxed (∼140 °C) for 7 h. The hot xylene solution (∼90 °C) was slowly added to methanol to precipitate PE-*g*-TEPA. The solid was further purified by a second precipitation from hot xylene into methanol. The solid was dried at 50 °C for 4 days and then in a vacuum oven at 50 °C for 20 h. Yield: 50.5 g (96%).

PIB-Coated Nanoparticles. Nanoparticles were prepared via modification of the method of Nakatani, Hijikara, and Ozawa.[9] Iron pentacarbonyl (21 g), PIB−TEPA (22 g of a 50 wt % solution in mineral oil), and kerosene (62 mL) were added to a 500-mL reaction flask fitted with a four-necked head carrying (1) a septum for the introduction of gases, (2) a lubricated bearing to accommodate the glass shaft of an overhead stirrer, (3) a thermocouple to monitor solution temperature, and (4) a dropping funnel and condenser cooled to −15 °C with a refrigerated circulating bath. The reaction mixture was deoxygenated by bubbling with argon for 20 min and then bubbled with ammonia for 20 min before the temperature was raised to 95 °C. The solution temperature was maintained at ∼95 °C (±5 °C) for 8 h, increased to 190 °C, and held there for 2 h. The reaction mixture was bubbled with ammonia (250 mL/min) and stirred throughout the reaction.

After cooling, the resulting black solution was added dropwise to 1.2 L of acetone/methanol (1:1) to precipitate the magnetic nanoparticles, together with any unbound dispersant. The thick black oil was purified by two additional precipitations, once from hexane (∼100 mL) into 1.5 L of acetone/methanol (3:1) and the second time from hexane into 1.5 L of acetone. The material was isolated, dissolved in hexane, and transferred to a round-bottomed flask. A rotary evaporator was used to remove hexane and then the material was further dried under vacuum while being heated (95 °C). The material was obtained as a sticky black solid at a yield of 13.75 g (81%). Other PIB-coated nanoparticles were prepared in a similar fashion.

PE-Coated Nanoparticles. These nanoparticles were prepared as described above for the PIB-coated material with the following modifications. PE−TEPA was used instead of PIB−TEPA and it was dissolved by heating the solvent (kerosene) to 95 °C while bubbling with argon. The heated solution was bubbled with ammonia before iron pentacarbonyl (10.5 g) was added from the dropping funnel. The reaction mixture, which gelled upon cooling, was diluted with 25 mL of toluene and heated before precipitation in 1.5 L of methanol. The solid was redissolved in hot toluene and then precipitated in 1.5 L of methanol. Drying under vacuum at 60 °C gave a black powder at a yield of 11.00 g (77%).

PS-Coated Nanoparticles. PS-coated nanoparticles were prepared in a manner similar to the PIB-coated materials described above with some modifications, which are illustrated in the following example. 1-Methylnaphthalene (62 mL) was used in place of kerosene and 11 g of PS-*g*-TEPA (M_n = 9000 g/mol) was used in place of PIB−TEPA. They were combined with 10.5 g of iron pentacarbonyl, and the reaction was conducted as described for the PIB-coated nanoparticles. Following the reaction, the material was isolated by precipitation in methanol and then further purified by a second precipitation from toluene into methanol. Drying under vacuum at 50 °C led to a black powder (72% yield). Other PS-coated samples were prepared in a similar fashion.

Results and Discussion

Dispersants. The dispersant serves to stabilize the growing particles and, thus, control the particle size. In addition, strongly bound dispersant would provide a protective polymer coating in a core−shell nanocomposite. The nature of the dispersant is of importance since the solution and solid state properties of the nanocomposite materials will reflect the properties of the dispersant. Material processing may be greatly simplified by the ability to cast films or to mold/extrude the material.

The dispersant may play an additional role by catalyzing iron pentacarbonyl decomposition. Nucleophilic solvents or polymers can facilitate disproportionation of metal carbonyls to give metal carbonyl anion complexes, which can be transformed to the metal upon heating.[12−14] Even nonnucleophilic polymers may aid the decomposition by combining with iron tetracarbonyl, the reactive intermediate formed by thermolysis of iron pentacarbonyl.[12] The polymer-bound carbonyl complex undergoes decomposition to metal faster than iron pentacarbonyl alone.

Nakatani et al.[9] found that PIB bearing tetraethylenepentamine (TEPA), a short polyethyleneimine chain, led to iron nitride nanoparticles of fairly uniform size. Presumably, TEPA was bound to the magnetic core, by adsorption to or chemical incorporation into the surface of the core, while the longer PIB chain stabilized the particles in the hydrocarbon solvent.

Following this precedent, the present work employed several different dispersants bearing TEPA groups. Three different types of dispersant, based on TEPA-functionalized polyethylene (PE), polyisobutylene (PIB), and polystyrene (PS), were investigated. PS and PIB are soluble in a variety of organic solvents while PE is soluble only in high boiling solvents (typically aliphatic and chlorinated hydrocarbons) at elevated temperatures. PS provides a rigid matrix at room temperature (T_g = 100 °C[24]) but one that can be melted and processed at temperatures above 100 °C. Both PE (T_g ∼ −125 °C) and PIB (T_g ∼ −73 °C) provide less rigid matrixes.[24] Despite its lower T_g, PE is generally tougher and more rigid than PIB, which tends to be soft and rubbery.

PIB−TEPA is a commercially available dispersant made by grafting maleic anhydride to the end of PIB chains, followed by reaction of the terminal anhydride with TEPA. The dispersant has a block copolymer structure. The PIB−TEPA dispersant used in this work was analyzed by size exclusion chromatography and found to have a molecular weight (M_n) of 4000 g/mol.

The PE−TEPA dispersant was formed by the reaction of maleic anhydride-grafted PE with TEPA in refluxing xylene. Under these conditions, an imide group is formed, and this was confirmed by FTIR analysis of a PE−TEPA film. Peaks were present for the imide (1701, 1769 cm^{-1}), but not for anhydride (1782, 1859 cm^{-1}) or carboxylic acid groups (1716 cm^{-1}). The dispersant will contain PE chains with no TEPA groups as well as those that have two or more TEPA chains because of the random nature of the maleic anhydride grafting process.

Preparation of Polystyrene−Tetraethylenepentamine Dispersants. Polystyrene dispersants bearing TEPA were synthesized by the two routes outlined in Scheme 1. In the first approach, conventional free-radical copolymerization of styrene and small amounts of 4-vinylbenzyl chloride (VBC) were used to produce random copolymers (PS−VBC), to which TEPA was

(24) Andrews, R. J.; Grulke, E. A. In *Polymer Handbook*, *4th*; Brandrup, J., Immergut, E. H., Grulke, E. A., Eds.; Wiley: New York, 1999; p. VI/193.

Scheme 1

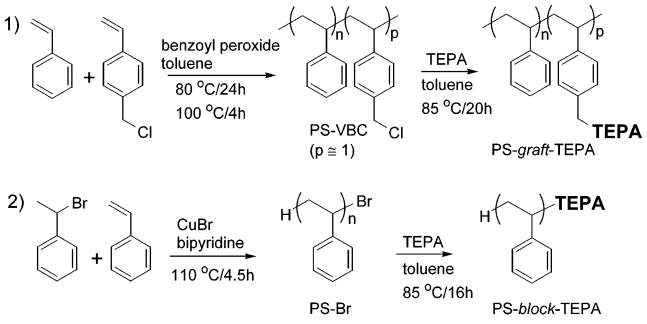

Table 1. Properties of PS−TEPA Dispersants

polymer	% yield	mol % TEPA[a]	M_n (g/mol)	M_w/M_n	T_g (°C)
PS-*g*-TEPA (3k)	90	2	3400	1.68	64
PS-*g*-TEPA (6k)	85	1	5700	1.6	85
PS-*g*-TEPA (9k)	69	1	9200	1.65	95
PS-*g*-TEPA (16k)	68	0.5	16300	1.83	93
PS-*b*-TEPA (8k)	82	1.4	7500	1.21	87
PS-*b*-TEPA (12k)	81	0.9	12400	1.21	89
PS-*b*-TEPA (19k)	60	0.5	19300	1.18	94

[a] Designed to yield dispersants with an average of one TEPA per chain.

added via reaction at the chloromethyl groups. The dispersant prepared by this route, PS-*g*-TEPA, consists of polystyrene main chains grafted with TEPA side chain(s). The VBC loading was such that an average of one TEPA unit per chain was obtained, and thus, the dispersants would have a polar head−hydrophobic tail structure. It should be noted that polystyrene chains bearing zero, two, or more TEPA units may also be formed.

Another dispersant architecture is accessible via atom transfer radical polymerization (ATRP).[25] ATRP is a controlled polymerization which gives narrow-disperse polymer chains capped with a labile end group, bromine in this case (Scheme 1). Substitution of this bromine with TEPA leads to PS-*b*-TEPA dispersants, block copolymers with PS chains connected at one end to single TEPA segments. The syntheses (via both conventional and ATRP routes) were designed to yield dispersants with a range of molecular weights.

The PS−TEPA dispersants were produced in good yields (Table 1). The graft dispersants (PS-*g*-TEPA) have molecular weights that range from M_n = 3400 g/mol to M_n = 16 300 g/mol, while the block dispersants (PS-*b*-TEPA) range from M_n = 7500 to M_n = 19 300 g/mol. The polymers produced via ATRP have much narrower molecular weights ranges (lower M_w/M_n), as expected.

The weight percent TEPA shown in the table is based on the reaction stoichiometry. Characterization of the polymers by nuclear magnetic resonance (NMR) spectroscopy showed the expected peaks including those characteristic of TEPA. The broad and overlapping peaks made it difficult to draw quantitative conclusions, but showed that TEPA was included in approximately the expected amount. Elemental analyses of several polymers also confirmed that the syntheses were successful. For instance, polystyrene (M_n = 12000 g/mol) produced by ATRP showed 0.8% Br vs the expected

(25) Patten, T. E.; Matyjaszewski, K. *Acc. Chem. Res.* **1999**, *32*, 895.

Scheme 2

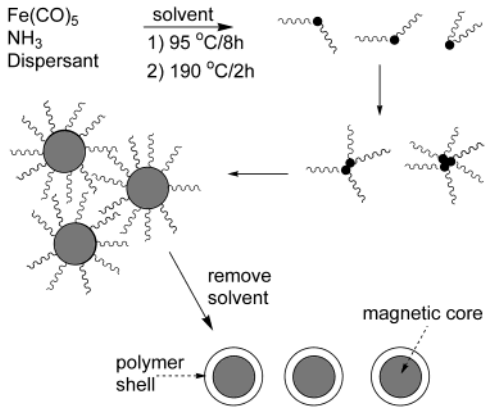

0.7%, and PS-*b*-TEPA (M_n = 7,500 g/mol) had 0.9% N, as expected.

The glass transition temperature (T_g) of the dispersants ranged from 64 to 95 °C (Table 1), lower than that for polystyrene itself ($T_g \approx$ 100 °C). This is likely due to both the low molecular weight of the samples and the presence of TEPA. In contrast to the polyisobutylene-based dispersant, the polystyrene-based dispersants have T_g values high enough to provide a rigid matrix at room temperature.

Polymer-Coated Nanoparticles. The preparation of polymer-coated nanoparticles, outlined in Scheme 2, was an adaptation of the method used by Nakatani, Hijikata, and Ozawa to prepare polyisobutylene-coated iron nitride (ϵ-Fe_3N) nanoparticles.[9,26] In their work, iron pentacarbonyl was thermally decomposed in the presence of a polymeric dispersant, ammonia, and kerosene. Ammonia was provided as the source of nitrogen required for the formation of iron nitride. The published method[9] involved a series of 3−6 heating cycles (90 °C/2 h and then 185 °C/2 h) in which excess iron pentacarbonyl was condensed into a reservoir before the high-temperature portion of each cycle and was then returned to the reactor at the beginning of the next cycle.

In the present work, iron pentacarbonyl was decomposed in the presence of a polymeric dispersant, ammonia, and a solvent; however, only a single heating cycle was used. The reaction mixture was held at 95 °C for 8 h, then heated to 190 °C, and held there for 2 h. Much of the iron pentacarbonyl is consumed during the temperature ramp. For reactions with PIB−TEPA and PE−TEPA dispersants, kerosene was used as the solvent, while those with PS−TEPA dispersants used 1-methylnaphthalene (1-MN; bp = 240 °C) or Decalin (bp = 190 °C).

The composite materials (magnetic nanoparticles plus unbound dispersant) were isolated from the reaction solvent by precipitation and then further purified by one or two additional precipitations. Black or gray solids were obtained with typical yields of ≈70% (Table 2). The solids, which ranged from sticky tars (PIB-coated) to powders (PS-coated), could be redispersed in solvents such as hexanes (PIB-coated) or toluene (PS-coated).

(26) Mamiya, H.; Nakatani, I. *J. Magn. Magn. Mater.* **1998**, *177−181*, 966; Mamiya, H.; Nakatani, I.; Furubayashi, T. *Phys. Rev. Lett.* **1998**, *80*, 177. Mamiya, H.; Nakatani, I. *J. Appl. Phys.* **1997**, *81*, 4733.

Table 2. Properties of Polymer−Iron Nanocomposites

dispersant[a]/$Fe(CO)_5$ (g)	wt % Fe[b]	% yield	particle diameter (nm)[c]	core diameter (nm)	T_g (°C)
PIB−TEPA/10.5	21	84	8 ± 1	3	
PIB−TEPA/10.5[d]	21	63	17 ± 3	13	
PIB−TEPA/21	35	81	12 ± 2	8	
PIB−TEPA/40.5	51	87	18 ± 2	14	
PIB−TEPA/60	61	87	20 ± 4	14	
PE−TEPA/10.5	21	77	16 ± 4	8.5	
PS-*g*-TEPA(9k)/10.5	21	72	∼24	∼18	91
PS-*g*-TEPA(16k)/10.5	21	68	∼25	∼20	94
PS-*g*-TEPA(3k)/10.5	21	70	∼28	∼22	75
PS-*g*-TEPA(6k)/10.5	21	79	∼30	∼24	66
PS-*b*-TEPA(12k)/10.5	21	71	∼35	∼30	80
PS-*b*-TEPA(8k)/10.5	21	64	∼37	∼32	87
PS-*b*-TEPA(8k)/10.5[e]	21	43	10 ± 2	4 ± 2	
PS-*b*-TEPA(19k)/10.5	21	87	∼50	∼45	81
PS-*g*-TEPA(3k)/40.5	51	69	∼45	∼40	84

[a] All preparations used 11 g of dispersant except where indicated. Solvent is kerosene for PIB−TEPA and PE−TEPA and 1-methylnaphthalene for PS−TEPA unless otherwise noted. [b] Weight % Fe expected from reaction stoichiometry. [c] Average diameter ± standard deviation measured for approximately 100 particles. [d] 1-Methylnaphthalene as reaction solvent. [e] Decalin as reaction solvent. Preparation with 5 g of PS-*b*-TEPA(8k).

Glass transition temperatures were measured for the PS-coated materials and one of the five PIB-coated materials. The PIB-coated material had a T_g of −59 °C, similar to that of pure PIB. T_g for the PS-coated samples fell between 66 and 94 °C. The composite materials, as produced, contain considerable fractions of unbound dispersant, and thus, it is not surprising that the materials exhibit T_g values similar to the dispersants from which they are made. The PS dispersants provide a rigid matrix that can be melted at easily accessible temperatures, which could simplify processing of the solids. The PS matrix might also allow the particles to be magnetically aligned at elevated temperature and then locked in place by cooling in the field.

The iron content measured by ICP-MS for the PS-coated materials was lower than that expected on the basis of reaction stoichiometry. Iron contents were found to range from 9 to 15 wt % for samples with a nominal 21 wt % iron, while 46% was found for the sample with a nominal 51 wt % iron. Similar information was gleaned from thermogravimetric analysis (TGA) of the PS-coated materials under an argon atmosphere. Rapid weight loss occurred above 350 °C and no further weight loss was observed above 600 °C. The residue consists principally of iron but iron oxide or iron nitride could also remain if present in the composite material. In addition, thermal decomposition of PS may leave some carbon residue. In each case the residual weight percent was lower than that expected for iron based on the reaction stoichiometry. Samples with an expected iron loading of 21% showed residual weight percent of 12.9−17.5% while the sample with an expected loading of 51% gave a residual weight percent of 47.3%. The lower than expected levels of iron shown by both ICP-MS and TGA are probably due to the loss of volatile iron pentacarbonyl during reaction and by the formation of an iron coating on the reactor walls.

Nanoparticle Morphology. Transmission electron microscopy (TEM) was used to characterize the nanocomposites. The materials prepared with either PE−TEPA and PIB−TEPA dispersants consisted of simple core−shell nanoparticles where the polymer shell is clearly visible (Figure 1). The particles produced in a given preparation are of fairly uniform size (Table 2), but they were larger than those produced by Nakatani et al. with similar reaction stoichiometry, albeit a different heating profile.[9] With the PIB dispersants, the particle size is determined, in part, by the iron pentacarbonyl loading, increasing from 8 ± 1 nm for a 1:1 iron pentacarbonyl/dispersant ratio to 20 ± 4 nm for a 5.5:1 ratio. The shell thickness is about 2 nm for the PIB-coated particles and about 4 nm for the PE-coated particles. Thus, PIB- and PE-coated nanoparticles with core diameters varying from about 4 to 15 nm were produced.

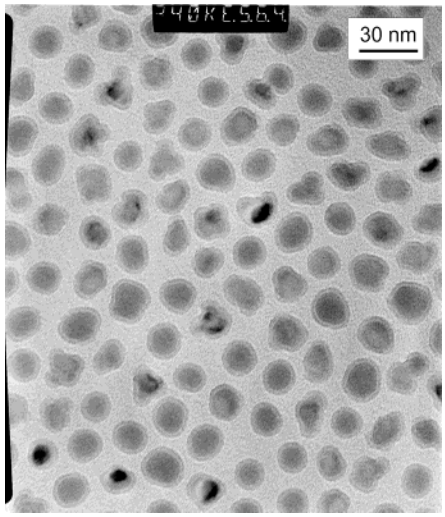

Figure 1. TEM image of PIB-coated nanoparticles made with 80 g of $Fe(CO)_5$ and 11 g of PIB−TEPA.

Preparations carried out with the PS−TEPA dispersants in 1-methylnaphthalene (1-MN) resulted in the formation of more complex structures (Figures 2−5), in addition to core−shell particles. Simple core−shell particles of ≈10−20 nm in diameter were present in most of the samples, but the bulk of the material in each case was comprised of larger, more complex particles, which ranged in size from 20 to 100 nm in diameter depending on the sample. These larger particles appeared to be agglomerates of smaller core−shell particles, as the polymeric shells extend into the particles, partially separating the cores within the complex aggregates. This indicates that core−shell particle formation was well advanced before agglomeration occurred. The particles, both simple and complex, bear strongly bound polymer coatings of 2−3-nm thickness. In view of the range of particle sizes formed for the PS-coated nanoparticles, the particle diameters given for PS-coated particles in Table 2 should be taken as an approximate particle size.

Clusters, loops, and strings containing anywhere from a few to thousands of the particles (Figures 2−5) were often observed in the TEM images. Magnetic interactions between the nanoparticles may cause the observed clustering.[10−12] Presumably, particles with a core diameter ≥20 nm have magnetic moments large enough to overcome the Brownian motion. Below this size, the particles may remain well dispersed in solution, leading

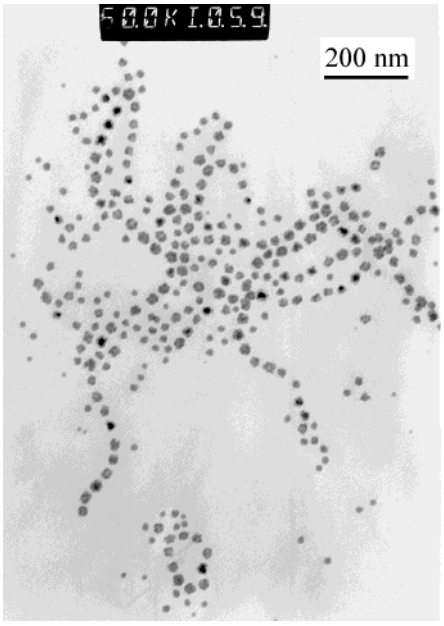

Figure 2. TEM image of PS-coated nanoparticles made with 10 g of $Fe(CO)_5$ and 11 g of PS-*g*-TEPA (9k).

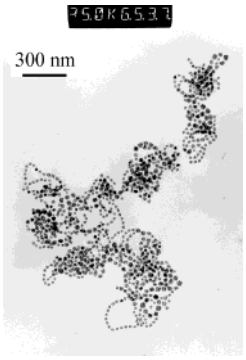

Figure 3. TEM image of PS-coated nanoparticles made with 10 g of $Fe(CO)_5$ and 11 g of PS-*g*-TEPA (3k).

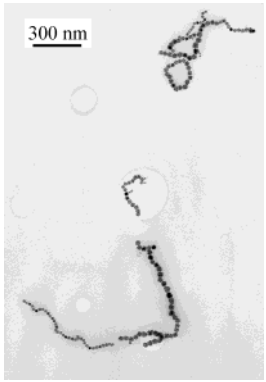

Figure 4. TEM image showing strings of PS-coated nanoparticles made from 10 g of $Fe(CO)_5$ and 11 g of PS-*g*-TEPA (16k).

to monolayers and free particles when deposited on the TEM grid.

Some other interesting structures are observed. Coils made from one or more particle strings were observed with one sample (Figure 5). In some instances, particle strings and loops were observed that were formed only of like-sized particles. For example, in Figure 4 one string near the bottom of the image is composed of 34 ± 3 nm in diameter particles while the neighboring

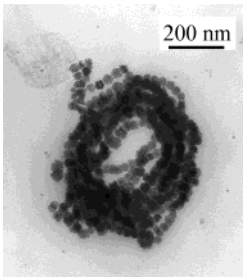

Figure 5. TEM image of a coil of PS-coated nanoparticles made from 10 g of $Fe(CO)_5$ and 11 g of PS-*b*-TEPA (8k).

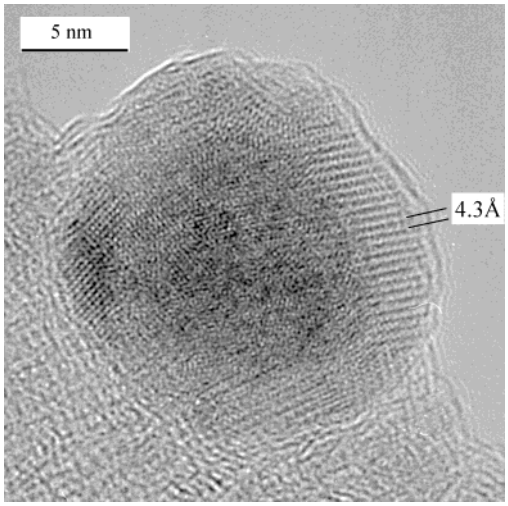

Figure 6. High-resolution TEM image of PIB-coated nanoparticles made with 60 g of $Fe(CO)_5$ and 11 g of PIB-TEPA. Lattice planes are visible in the shell region of the particles.

string contains particles of 22 ± 1 nm in diameter. It may be that the balance of magnetic and thermal forces allows progressively smaller particles to cluster as the reaction mixture cools and these strings/loops remain intact when the sample is redispersed prior to TEM analysis.

Another feature present in Figure 1, and in many of the other TEM images of the polymer-coated nanoparticles, is that the particles are not in contact with their nearest neighbors. During preparation of the TEM sample, solvent-dispersed particles with swollen shells may be deposited in a close-packed array on the carbon support. Solvent evaporation causes the polymer shells to contract and withdraw toward the cores which retain their relative positions. The spacing between two adjacent cores reveals the thickness of the solvent-swollen shells and provides evidence that the shell is indeed composed of polymeric material, which is tightly bound to the core.

Several of the nanoparticle materials were investigated by high-resolution TEM. While small crystalline regions were observed within the cores, in no case did the core consist of a single crystal. A surprising observation was made when the PIB-coated nanoparticles were investigated with high-resolution TEM. Lattice fringe planes, indicative of crystalline regions, were observed in portions of the nanoparticles comprised of only the shell (Figure 6). The large crystallite in Figure 6 is ≈10 nm in length. While PIB is normally a rubbery, amorphous solid, it is known to crystallize when extended to 10 or more times its relaxed length.[27] The observed

lattice spacings (4.4, 4.1, 2.8, 2.7, 2.4, 2.3, 2.2, and 1.9 Å) were similar, but not identical, to those of crystalline-stretched polyisobutylene.[27] The dense packing caused by binding of the dispersants to the core may serve similarly to stretch and align the chains and allow crystallization. Shorter alkyl chains are known to align or crystallize upon binding to surfaces.[28]

Lattice planes were also visible in the shell of the PS-coated nanoparticles but were not as pronounced as with the PIB-coated samples. Since the crystallization of atactic PS is not possible, the lattice fringes ($d \sim 1.8$, 2.3, 4.3 Å) may reflect ordering or alignment of the PS chains but not proper crystallization.

The appearance of larger complex particles with the change from polyisobutylene- to polystyrene-based dispersants indicates that the latter are somewhat less effective at particle stabilization in solution. Factors such as dispersant chain length, dispersant structure, and the solvent−dispersant interaction will play important roles. The importance of dispersant structure has been noted in small molecule systems where stable dispersions of iron particles were obtained with oleic acid (octadec-9-enoic acid) but not stearic acid (octadecanoic acid), which differ only by the presence of a double bond.[15] It had been expected that block dispersants (PS-*b*-TEPA) might prove more efficient at particle stabilization as the full length of the PS chain might project into the solvent and provide greater steric stabilization. However, complex particles were formed with dispersants of both block and graft architectures, and in fact, the average particle size and the fraction of complex particles was generally lower for the PS-*g*-TEPA dispersants.

Solvent Effects on Nanoparticle Morphology. The importance of the dispersant−solvent interactions was demonstrated by two experiments. A change in reaction medium from kerosene to 1-methylnaphthalene (1-MN) for a preparation with PIB−TEPA caused a particle size increase from 8 ± 1 to 17 ± 3 nm (Table 2). A measure of the polymer−solvent interaction can be obtained by comparing the solvent parameters for PIB ($\delta = \sim 16$ Mpa$^{1/2}$), kerosene (~15) and 1-MN (21.2).[29] Poorer solvation of the PIB chains in 1-MN will lead to a more compact polymer coil and, thus, weaker steric stabilization of the growing particle. This may cause nucleation of particle precursors at an earlier stage of the reaction or an extended particle growth phase before the polymer chains hinder the addition of more core material and particle growth ceases.

The solubility parameters for the PS/1-MN system, $\delta = \sim 18$ Mpa$^{1/2}$ for PS and 21.2 Mpa$^{1/2}$ for 1-MN,[29] reveal some mismatch between solvent and polymer. A dramatic change in particle size and morphology was obtained when particles were prepared in Decalin ($\delta =$ 18 Mpa$^{1/2}$). Particles prepared with PS-*b*-TEPA(8k) in 1-MN were large and complex (~37 nm in diameter, see Figure 5) while those prepared in Decalin were simple

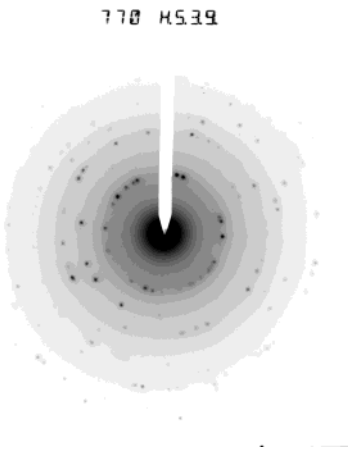

Figure 7. Electron diffraction pattern obtained from PS-coated nanoparticles made with 10 g of $Fe(CO)_5$ and 11 g of PS-*b*-TEPA (8k).

core−shell particles of fairly uniform size (diameter = 10 ± 2 nm). Thus, the solvent−polymer interaction plays a key role in determining the particle size and structure, and the polystyrene-based dispersants seem particularly sensitive to this parameter. Further experiments aimed at a better understanding of the solvent/polymer effects on particle size and structure are underway.

Nanoparticle Composition. X-ray powder diffraction analysis was conducted on several of the nanocomposites. Most of the samples did not display any peaks, likely due to the high content of amorphous polymer and the small particle sizes. One sample with higher iron loading displayed a single peak at $2\theta = 44.7°$, which corresponds to metallic iron (α-Fe).

Electron diffraction was used to probe the composition and crystallinity of the core since it is possible to focus on groups of particles free from interference by the unbound amorphous polymer. Selected area electron diffraction patterns were collected from freshly prepared samples of the nanocomposites. With large particles, distinct patterns (Figure 7) were obtained, while smaller particles gave weak patterns consisting of faint rings. The *d* spacings measured from the patterns (2.06, 1.47, 1.18, 1.02, and 0.90 Å; error ~1−2%) and the relative intensities of the diffraction rings/spots were consistent with metallic iron (α-Fe: 2.03, 1.43, 1.17, 1.01, and 0.91 Å).[30] Thus, under our reaction conditions ammonia is not utilized to form iron nitride (ϵ-Fe_3N) as had been observed previously.[9]

The lack of nitrogen required for an iron nitride composite material was confirmed by elemental analysis of three of the PS-coated materials. In each case, the nitrogen content (0.78, 0.75, and 0.49%) was close to that expected from the TEPA groups of the dispersant alone (0.59, 0.79, and 0.31%), but lower than that expected for iron nitride and the TEPA groups (4.24, 1.65, and 0.80%).

The electron diffraction patterns from some samples contained a faint ring ($d = \sim 2.55$ Å), which corresponds to γ-Fe_2O_3/Fe_3O_4, and indicates that some minor oxidation occurred during preparation or handling of the materials. TEM samples of the PIB-coated materials

(27) Fuller, C. S.; Frosch, C. J.; Pape, N. R. *J. Am. Chem. Soc.* **1940**, *62*, 1905; Liquori, A. M. *Acta Crystallogr.* **1955**, *8*, 345. Tanaka, T.; Chatani, Y.; Tadokoro, H. *J. Polym. Sci., Polym. Phys. Ed.* **1974**, *12*, 515.

(28) Schlotter, N. E.; Porter, M. D.; Bright, T. B.; Allara, D. L. *Chem. Phys. Lett.* **1986**, *132*, 93; Ahn, S. J.; Son, D. H.; Kim, K. *J. Mol. Struct.* **1994**, *324*, 223.

(29) Grulke, E. A. In *Polymer Handbook, 4th*; Brandrup, J., Immergut, E. H., Grulke, E. A., Eds.; Wiley: New York, 1999; p VII/675.

(30) *Powder Diffraction File*; International Centre for Diffraction Data: Swarthmore, PA, 1988; File # 6-696.

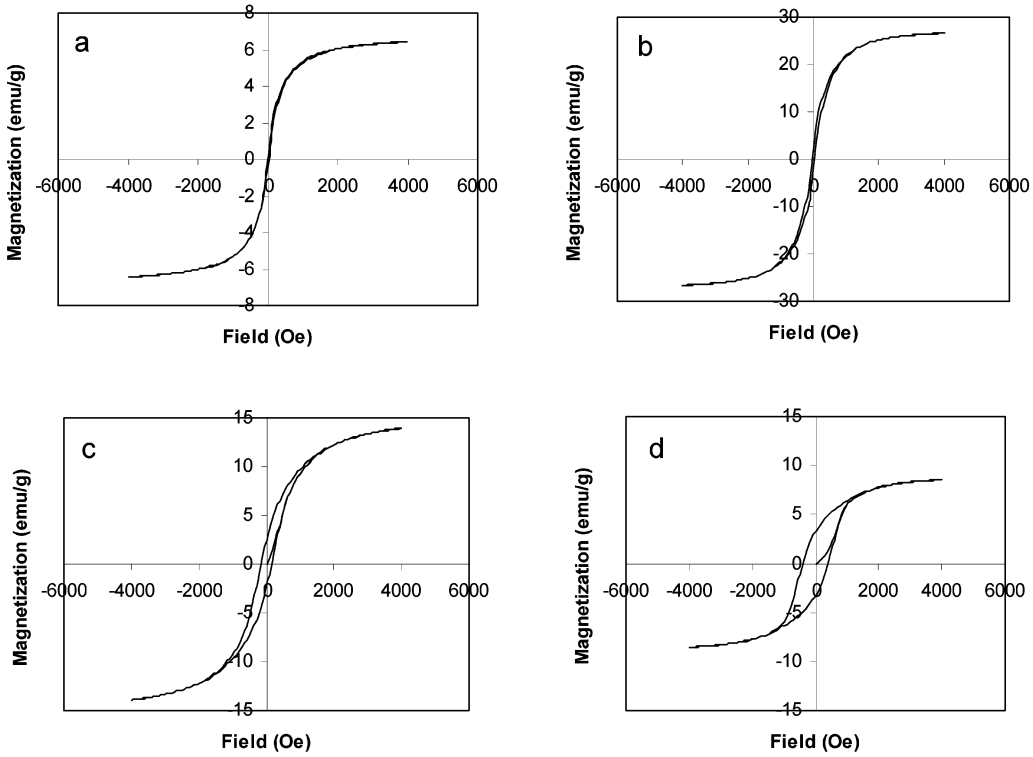

Figure 8. Magnetization vs applied field for the following: (a) PIB-coated nanoparticles made with 20 g of $Fe(CO)_5$ and 11 g of PIB-TEPA. Core diameter = 13 nm. (b) PIB-coated nanoparticles made with 40 g of $Fe(CO)_5$ and 11 g of PIB−TEPA. Core diameter = 14 nm. (c) PS-coated nanoparticles made from 10 g of $Fe(CO)_5$ and 11 g of PS-*b*-TEPA (12k). Core diameter ∼30 nm. (d) PS-coated nanoparticles made from 10 g of $Fe(CO)_5$ and 11 g of PS-*g*-TEPA (16k). Core diameter ∼20 nm.

exposed to the atmosphere for several months showed diffraction patterns consistent with γ-Fe_2O_3/Fe_3O_4, revealing that oxidation of the iron core had occurred. Controlled oxidation of the initially formed nanoparticles, thus, provides a possible route to polymer-coated iron oxide nanoparticles.[15]

Electron diffraction patterns obtained from a freshly prepared TEM sample of the PE-coated material showed faint rings with *d* spacings best indexed by γ-Fe_2O_3/Fe_3O_4. Oxidation may have occurred during preparation of the TEM sample. The PE−TEPA dispersant is soluble only in hot solvents, and it was necessary to heat the PE-based nanocomposite in toluene at ≥100 °C for an extended period to prepare a sample for TEM analysis. Samples of the PS-coated material exposed to the atmosphere for a month did not show evidence of oxidation to iron oxides.

Magnetic Properties. Magnetic hysteresis loops, as shown in Figure 8, were measured on solid samples at 290 K with a SQUID magnetometer. The saturation magnetization (σ_s), coercivity (H_c), and remanence ratio (σ_r/σ_s) are given in Table 3. σ_s was determined from the intercept of a magnetization vs 1/field plot for the data at high field.

σ_s varies from 0.9 to 37.8 emu/g for the nanocomposite materials as prepared, where the highest values are associated with the samples with the highest iron loading. When expressed per gram of iron in the nanocomposites, σ_s, ranges from ∼8 to ∼140 emu/g of Fe. The magnetization is lower than that for crystalline bcc iron (222 emu/g)[31] but approaches that reported for amorphous iron (156 emu/g (0 K)).[32] Magnetizations lower than that of crystalline bcc iron have been observed for a number of iron nanoparticle materials.[12,15,33] The reduced magnetizations may be related to the nature of the core or core surface. High-resolution TEM revealed that the nanoparticle cores were not single crystals, but were perhaps polycrystalline or a mixture of crystalline and amorphous material. The crystalline nature of the magnetic material will have a pronounced effect on the magnetization. Kataby et al.[33]

Table 3. Summary of Magnetic Properties

dispersant	wt % Fe[a]	σ_s (emu/g)	H_c (Oe)	σ_r/σ_s	core diameter (nm)
PIB−TEPA	21	0.92	0	0	3
PIB−TEPA/1-MN[b]	21	3.6	0	0	13
PIB−TEPA	35	6.9	0	0	8
PIB−TEPA	51	28	34	0.065	14
PIB−TEPA	61	37.8	66	0.109	14
PS-*g*-TEPA(9k)	21	7.6	198	0.29	∼18
PS-*g*-TEPA(16k)	21	9.3	390	0.34	∼20
PS-*g*-TEPA(3k)	21	13.2	254	0.3	∼22
PS-*g*-TEPA(6k)	21	10.4	232	0.25	∼24
PS-*b*-TEPA(12k)	21	15.6	162	0.15	∼30
PS-*b*-TEPA(8k)	21	15.9	214	0.19	∼32
PS-*b*-TEPA(19k)	21	16.9	204	0.11	∼45
PS-*g*-TEPA(3k)	51	29.3	74	0.11	∼40
PE-*g*-TEPA	21	1.8	0	0	8
Fe	100	222[c]			

[a] Weight percent Fe expected from feed ratios. [b] 1-Methylnaphthalene used as reaction solvent. [c] Craik, D. *Magnetism: Principles and Applications*; Wiley: Toronto, 1995; p 404.

(31) Craik, D. *Magnetism*: *Principles and Applications*; Wiley: Toronto, 1995; p 404.
(32) Grinstaff, M. W.; Salamon, M. B.; Suslick, K. S. *Phys. Rev. B* **1993**, *48*, 269.
(33) Kataby, G.; Cojocaru, M.; Prozorov, R.; Gedanken, A. *Langmuir* **1999**, *15*, 1703.

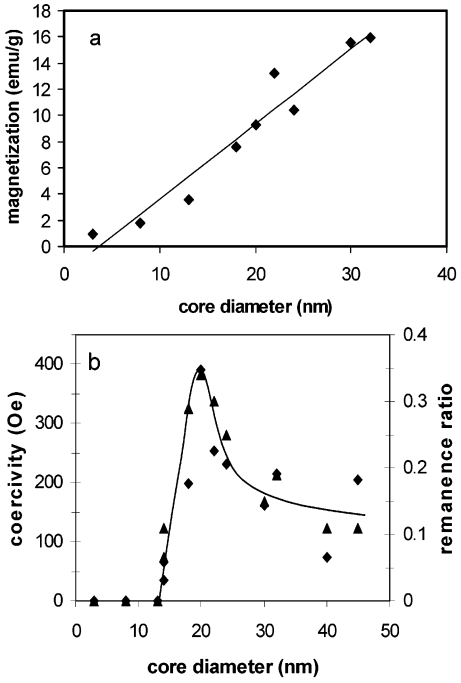

Figure 9. Effect of core size on magnetic properties: (a) magnetization vs core diameter for nanoparticle samples with nominal iron content of 21 wt %; (b) coercivity (◆) and remanence (▲) vs core diameter. Trendline is for visualization purposes only.

investigated a number of surfactant-coated iron nanoparticles and found that the nature of the group bound to the nanoparticle surfaces had a dramatic effect on the magnetization.

The magnitude of σ_s is also affected by particle size. The samples with a nominal iron content of 21% exhibit σ_s values across a considerable range. For these samples, the observed σ_s correlates well with the core size (Figure 9a). This relationship has been observed previously[5,21,22] and has been attributed to the role of the particle surface. With smaller particles a significant fraction of the atoms lie at or near the core/shell interface. Crystalline disorder within the surface layer, effects such as pinning or canting, or reaction of surface atoms with TEPA, ammonia, or oxygen may create a magnetically dead layer and lead to a dramatic decrease in the magnetization.[22,33,34] For the PE-coated material, core oxidation as detected during TEM analysis may also contribute to the reduced magnetization.

Most of the solid materials exhibited hysteresis at room temperature, as displayed in Figure 8c,d. The materials with the smallest particle sizes were superparamagnetic[35] at room temperature (Figure 8a). The switch from ferromagnetic to superparamagnetic behavior for these materials occurs at ∼13 nm. For example, the magnetization curve for the PIB-coated sample with a mean core diameter of 14 nm (Figure 8b) displays the onset of ferromagnetic behavior with a small nonzero coercivity (34 Oe) and remanence ratio (6.5%). The changeover from superparamagnetism to ferromagnetism at ∼13 nm is in good agreement with previous reports which give a critical diameter of 12.5 nm for spherical iron particles.[5,36]

As the core size increases above 13 nm, the coercivity and remanence ratio increase and go through a maximum (H_c = 390 Oe; remanence ratio = 34%) at a core diameter of ∼20 nm (Figure 9b). Coercivity maxima have been reported for iron particles at 13[37] and 25 nm,[5] and the present results are in accordance with these values.

The maximum in the coercivity vs particle size relationship may result from a change in the demagnetization mechanism from domain wall migration to coherent rotation, which accompanies a switch from multiple- to single-domain particles as the size decreases.[2,5] The barrier to coherent magnetization rotation is proportional to particle volume, which would account for the rapid increase in coercivity between 13 and 20 nm. Above 20 nm, the coercivity falls, perhaps as it becomes easier to move domain walls, which are predicted to be on the order of 30−50-nm-thick for iron.[38,39]

Coercivity maxima have also been observed for thin iron films.[38,40] The maxima are thought to be due to magnetic phase transitions that accompany a change in crystal structure as the film thickness is varied.

The materials isolated following particle synthesis contain substantial amounts of unbound dispersant but this can be removed to produce a more concentrated magnetic material. When the composite material is dispersed in a good solvent for the polymer, it is possible to settle out, by gravity or via centrifugation, the magnetic nanocomposite. This process is most easily accomplished for those materials with larger particle sizes where particle clustering aids settling. Materials containing small particles remain dispersed even when centrifuged.

The material prepared with PS-*g*-TEPA(16k) (core diameter ∼20 nm) was dispersed in toluene and centrifuged to yield a concentrated fraction equal to ∼15% of the initial mass. σ_s for the concentrated material increased 7-fold (66.7 vs 9.3 emu/g), while M_s increased 10-fold (∼120 vs ∼11 emu/mL). The M_s increase is more pronounced because the density of the magnetic composite increases following settling.

During the preparation of one sample of PIB-coated nanoparticles, some material settled to the bottom of the reactor while some remained dispersed in the kerosene solvent along with any unbound dispersant. The two fractions were collected and purified separately before analysis. The two fractions showed no significant difference in particle size as measured by TEM, and the coercivities and remanence ratios were found to be similar; however, the settled fraction had a saturation magnetization more than 3 times that of the dispersed fraction (75.4 vs 21.3 emu/g). Thus, higher magnetizations can be obtained by removing unbound dispersant from the initially prepared material.

(34) Mollard, P.; Germi, P.; Rousset, A. *Physica B+C (Amsterdam)* **1977**, *86−88*, 1393.
(35) Cullity, B. D. *Introduction to Magnetic Materials*; Addison-Wesley: Reading, MA, 1972; p 410.
(36) Bean, C. P.; Livingston, J. D. *J. Appl. Phys.* **1959**, *30*, 120S.
(37) Luborsky, F. E. *J. Appl. Phys.* **1961**, *32*, 171S.
(38) We wish to thank a referee for this suggestion.
(39) Craik, D. *Magnetism*: *Principles and Applications*; Wiley: Toronto, 1995; p 97. Cullity, B. D. *Introduction to Magnetic Materials*; Addison-Wesley: Reading, MA, 1972; p 291.
(40) Berger, A.; Feldmann, B.; Zillgen, H.; Wuttig, M. *J. Magn. Magn. Mater.* **1998**, *183*, 35. Bader, S. D.; Li, D.; Qiu, Z. Q. *J. Appl. Phys.* **1994**, *76*, 6419.

The slope of the magnetization curve near $\sigma = 0$ is sometimes used to calculate a "magnetic" particle diameter for materials which are superparamagnetic.[21,22] The slope is related to the particle diameter through the following relationship,

$$d_{\mathrm{mag}} = \left(\frac{18kT\left(\frac{\mathrm{d}\sigma}{\mathrm{d}H}\right)_0}{\pi\rho{\sigma_{\mathrm{s}}}^2} \right)^{1/3}$$

where k is the Boltzmann constant, T is the temperature in Kelvin, $(\mathrm{d}\sigma/\mathrm{d}H)_0$ is the slope of the magnetization curve near $\sigma = 0$, ρ is the sample density, and σ_{s} is the saturation magnetization.

Magnetic diameters were calculated for the four samples which proved to be superparamagnetic. Sample densities were estimated by taking the relative contributions of polymer (density = 1 g/mL) and iron (7.8 g/mL). A value for the saturation magnetization was obtained by scaling the bulk iron value (222 emu/g) by an estimate of the iron content of the sample. Magnetic diameters of approximately 4, 9, 10, and 14 nm were obtained, which is in reasonable agreement with the core diameters of 3, 8, 8, and 13 nm, respectively, as measured by TEM.

Conclusion

Magnetic materials comprised of polymer−iron nanoparticle composites have been prepared by the thermal decomposition of iron pentacarbonyl in the presence of ammonia and several types of polymeric dispersants. The nanoparticles consist of metallic cores, each of which is coated with a strongly bound polymer layer. The polyisobutylene- and polyethylene-based dispersants lead to more uniform particle sizes and the materials are composed principally of individual core−shell particles. Large, complex particles, formed by the aggregation of smaller particles, as well as simple core−shell particles were obtained with polystyrene-based dispersants in 1-methylnaphthalene. Aggregation leading to complex particles was found to be due to a mismatch between the solubility parameters of the dispersant and the reaction solvent. When the solvent was better matched with the solubility parameter of polystyrene, simple core−shell nanoparticles of fairly uniform size were obtained.

Electron diffraction reveals that the core material is iron, which is in contrast to the iron nitride cores observed in previous work with PIB−TEPA dispersants. High-resolution TEM revealed highly ordered or crystalline regions within the polymer shell, possibly due to dense packing of the strongly bound dispersant chains. Magnetic interactions between particles cause secondary structures such as clusters, coils, loops, and strings of particles to be formed.

The nanocomposites can be dispersed in organic solvents or cast as films. The polystyrene−iron composites are rigid solids at room temperature but can be melted at convenient temperatures (e.g., 65−100 °C).

The nanoparticle composites show a range of magnetic behavior. Samples with the smallest particles proved to be superparamagnetic but their saturation magnetizations were low. For materials with larger particle sizes, hysteresis was observed and the materials possessed larger magnetizations. The magnetization was correlated with the particle size where samples with larger particles showed higher magnetizations. As expected, those samples with higher iron contents, whether produced by using higher iron pentacarbonyl loadings or by removing unbound polymer dispersant, showed the highest magnetization.

Acknowledgment. We wish to acknowledge the financial support of the Natural Sciences and Engineering Research Council of Canada. We wish to thank Dr. Graeme Luke for helpful discussions.

CM020126Q